Hindawi
Shock and Vibration
Volume 2019, Article ID 8120569, 12 pages
https://doi.org/10.1155/2019/8120569

Research Article

Study on the Dynamic Problems of Double-Disk Rotor System Supported by Deep Groove Ball Bearing

Yang Liu,[1] **Jiyuan Han**,[1] **Siyao Zhao**,[1] **Qingyu Meng**,[1] **Tuo Shi**,[2] **and Hui Ma**[1]

[1]*School of Mechanical Engineering and Automation, Northeastern University, Shenyang 110004, China*
[2]*Sichuan Aerospace Fenghuo Servo Control Technology Corporation, Sichuan 611130, China*

Correspondence should be addressed to Yang Liu; liuyang1982@mail.neu.edu.cn

Received 6 November 2018; Revised 23 January 2019; Accepted 7 February 2019; Published 26 February 2019

Academic Editor: Francesco Franco

Aiming at the analysis of the dynamic characteristics of the rotor system supported by deep groove ball bearings, the dynamic model of the double-disk rotor system supported by deep groove ball bearings was established. In this paper, the nonlinear finite element method is used combined with the structural characteristics of deep groove ball bearings. Based on the nonlinear Hertz contact theory, the mechanical model of deep groove ball bearings is obtained. The excitation response results of the rotor system nodes are solved by using the Newmark-β numerical solution method combined with the Newton–Raphson iterative method. The vibration characteristics of the rotor system supported by deep groove ball bearings are studied deeply. In addition, the effect of varying compliance vibration (VC vibration) caused by the change in bearing support stiffness on the dynamics of the system is considered. The time domain and frequency domain characteristics of the rotor system at different speeds, as well as the influence of bearing clearance and bearing inner ring's acceleration on the dynamics of the rotor system are analyzed. The research shows that the VC vibration of the bearing has a great influence on the motion of the rotor system when the rotational speed is low. Moreover, reasonable control of bearing clearance can reduce the mutual impact between the bearing rolling element and the inner or outer rings of the bearing and reduce the influence of unstable bearing motion on the vibration characteristics of the rotor system. The results can provide theoretical basis for the subsequent study of the nonlinear vibration characteristics of the deep groove ball bearing rotor system.

1. Introduction

Rolling bearing rotor system is the core of large rotating machinery, and it is widely used in electricity, chemicals, aviation and ships, and other important industries. The stiffness of the rolling bearing has strong time-varying characteristics and nonlinear characteristics under complex operating conditions such as variable load, which is usually the main source of nonlinearity of rolling bearing rotor system [1]. Deep groove ball bearing is one of the most widely used traditional shaft support parts, so it is of great significance to study its influence on the shaft system's dynamic characteristics.

In recent years, the research on the dynamic behavior of the rotor system supported by rolling bearing has been an important subject of many scholars. In the bearing rotor model of a rotating machine, the bearing seat that supports the circular motion of the rotor is always simplified to a rigid body, and the bearing can be simplified as a parallel combination of spring and damper. Then, the dynamic behavior of the rotor system is studied by solving the differential equations of the system [2, 3]. Fukata et al. [4] and Mevel and Guyader [5] studied the dynamic behavior of the rotor system under parametric excitation caused by the change of bearing stiffness. Cong et al. [6] established a two-degree-of-freedom bearing rotor system and studied the fault response of rolling bearings based on the assumptions of Jeffcott's rotor. Kim and Noah [7] studied the nonlinear characteristics of bearing clearance but did not involve the research on varying compliance vibration of system. Zhou and Chen [8] established a dynamic model of 2-DOF aero-engine double rotor rolling bearing casing coupling system based on the

study of Cong. Although the study of Tiwari et al. [9] has taken into account the bearing clearance and the variable stiffness of the system, the analysis of the influence of the bearing structure parameters on the system dynamics is not sufficient. Moreover, due to the existence of the fault, the analysis of the vibration characteristics of rolling bearings can be affected to a certain extent. El-Saeidy [10] established a stiffness matrix model of 5-DOF rigid spindle rotor angular contact ball bearing to study the time-varying stiffness. The results show that the time-varying stiffness of the bearing cannot be neglected when the bearing rotor model is established. In the past, few literatures have studied the factors affecting the change of bearing stiffness, or the influence of different bearing stiffness on the rotor system's dynamic characteristics.

Based on the structural characteristics of deep groove ball bearings, considering the factors such as centrifugal force, gyro moment, bearing ball count, and bearing clearance, a nonlinear model of deep groove ball bearings was established. The finite element model of deep groove ball bearing double-disk rotor system is established by integrating the subcomponent model of bearing rotor system. Then, the Newmark-β numerical solution method and Newton–Raphson iteration are used to solve the excitation response results of the rotor system's nodes. The model can simulate the dynamic behavior of the rotor when it is under the load. The dynamic characteristics of the rotor system are analyzed by using the spectrogram, the Poincaré section, the time domain chart, and so on. The time domain and frequency domain characteristics with the variable stiffness and different rotational speeds are studied. The effects of bearing clearance, bearing inner ring acceleration, and other parameters on the dynamic behavior of the rotor system are discussed.

2. Rotor System Dynamics Model

The double-disk rotor system supported by deep groove ball bearings has 16 nodes, divided into 15 shaft segments. As presented in Figure 1, the points in the figure is the shaft segment's key nodes, and the number indicates the corresponding node number. The coupling position is on the shaft section 1. Two disks with diameters of 60 mm are located at shaft section 12 and shaft section 7, respectively, and two deep groove ball bearings are located on the nodes 4 and 15, respectively. The specific parameters of the shaft sections are shown in Table 1.

Rotor system shaft section is simulated by Timoshenko beam element. To highlight the main problem, only the two end nodes (A and B) in the beam element are applied. In addition, the radial deformation of the nodes in the model is much larger than the axial deformation, and the magnitude difference is huge, so the axial deformation and torsional deformation are ignored. The axis segment diagram is shown in Figure 2.

The node A and node B in the Timoshenko beam element have 4 degrees of freedom. x_A, y_A, θ_{xA}, and θ_{yA} are the displacements and rotation angles of node A in the X and Y directions, respectively. x_B, y_B, θ_{xB}, and θ_{yB} are the displacement and corner of node B in X and Y directions, respectively. The x-axis and the y-axis are horizontal and vertical, respectively. The displacement vector of the Timoshenko beam element is $\mathbf{u} = [x_A, y_A, \theta_{xA}, \theta_{yA}, x_B, y_B, \theta_{xB}, \theta_{yB}]^T$.

2.1. Deep Groove Ball Bearing Model. As shown in Figure 3, O_1 is the bearing geometric center and O_2 is the rotation center of the bearing. Due to the continuous periodic variation of the deep groove ball bearing's total stiffness, the system will produce variable stiffness vibration, that is, VC vibration. The vibration is the parametric excitation and its frequency is the bearing ball's passing frequency.

In this paper, the outer ring of the deep groove ball bearing is fixed on the bearing seat, and the inner ring is fixed on the rotating shaft. The bearing balls are equidistantly arranged between the inner and outer raceways, and the movement of the bearing balls in the raceway is pure rolling. Bearing outer ring and bearing seat are in a quiescent state in Reference [11, 12]. The contact between the bearing's inner and outer rings with the rolling element conforms to the nonlinear Hertz contact theory. According to the nonlinear Hertz contact theory, the contact pressure F_j generated by the rolling contact between the jth ball and the raceway can be obtained. At the same time, considering that only the normal positive pressure can be generated between the ball and the raceway, the force will be generated only when the distance C between O_1 and O_2 is greater than the bearing clearance r_0, that is: $\delta_j = x\cos\theta_j + y\sin\theta_j - r_0 > 0$. The expression of the contact pressure can be obtained by using the Heaviside function H as follows:

$$\begin{aligned} F_j &= c_b\delta^{3/2} \\ &= c_b\left(x\cos\theta_j + y\sin\theta_j - r_0\right)^{3/2} \\ &\quad \times H\left(x\cos\theta_j + y\sin\theta_j - r_0\right), \end{aligned} \tag{1}$$

where c_b is the Hertz contact stiffness and is related to the type and shape of the contact material. θ_j is the position where the jth rolling element of the bearing is moved, $\theta_j = \omega_c \times t + 2\pi \times (j-1)/N_b$, $j = 1, 2, \ldots, N_b$, N_b is the number of rolling elements, and ω_c is the bearing cage rotation speed, $\omega_b = \omega \times r/(R+r)$. ω is the rotor rotation speed, and ω_{VC} is the passing frequency of the bearing rolling element, $\delta_j = x\cos\theta_j + y\sin\theta_j - r_0 > 0$.

The component of F_j in the X and Y directions is

$$\begin{cases} F_{jx} = F_j\cos\theta_j, \\ F_{jy} = F_j\sin\theta_j. \end{cases} \tag{2}$$

Bearing forces produced by the rolling bearings are

$$\begin{cases} F_{gx} = \sum_{j-1}^{N} F_{jx} = \sum_{j-1}^{N} F_j\cos\theta_j, \\ F_{gy} = \sum_{j-1}^{N} F_{jy} = \sum_{j-1}^{N} F_j\sin\theta_j. \end{cases} \tag{3}$$

The specific parameters of the deep groove ball bearings are listed in Table 2.

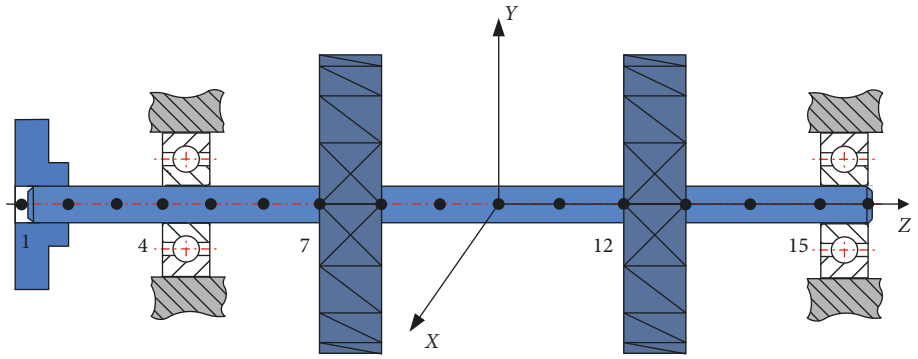

Figure 1: Rotor system dynamics mode.

Table 1: Shaft section parameters of rotor system.

Attributes	Data														
Shaft section number	1	2	3	4	5	6	7	8	9	10	11	12	13	14	15
Length (mm)	20	20	20	6	20	20	10	20	20	20	20	10	20	20	6
Diameter (mm)	28	10	10	10	10	10	60	10	10	10	10	60	10	10	10

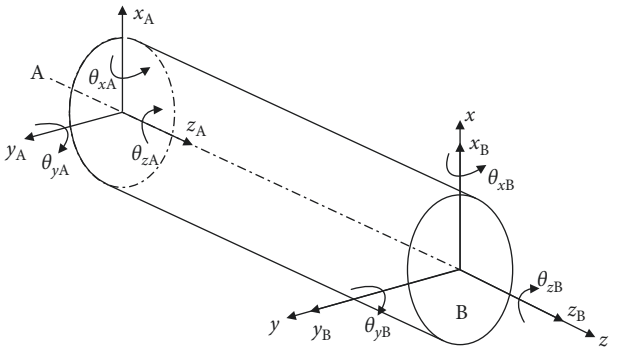

Figure 2: Timoshenko beam unit.

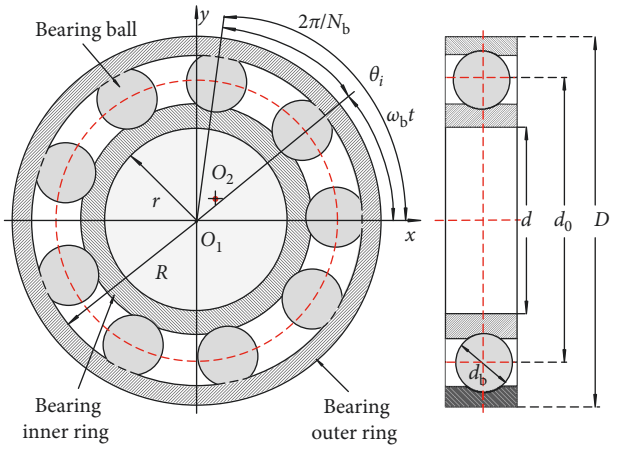

Figure 3: Bearing structure diagram.

Table 2: Bearing parameters.

Bearing type	Inner radius r (mm)	Outer radius R (mm)	Width B (mm)	Contact stiffness C_b (N/m$^{3/2}$)	Number of balls N_b	Clearance r_0 (μm)	Center distance d_0 (mm)
61900	5	10	6	13.34×10^9	9	0–45	16.45

2.2. Rotor System Dynamics Equation. In this paper, the finite element method is used to establish the dynamic model of deep groove ball bearing double-disk rotor system under rotational coordinates. The generalized coordinates of the rotor system in fixed and rotational coordinates are $\mathbf{u}_s$ and $\boldsymbol{u}$, respectively. The relationship between the two coordinates is shown in the following equation:

$$\mathbf{u}_s = \mathbf{T}\mathbf{u}, \tag{4}$$

where $\mathbf{T}$ is the transfer matrix, as follows:

$$\mathbf{T} = \begin{bmatrix} \cos\omega t & \sin\omega t & 0 & 0 & 0 & 0 & 0 & 0 \\ -\sin\omega t & \cos\omega t & 0 & 0 & 0 & 0 & 0 & 0 \\ 0 & 0 & \cos\omega t & \sin\omega t & 0 & 0 & 0 & 0 \\ 0 & 0 & -\sin\omega t & \cos\omega t & 0 & 0 & 0 & 0 \\ 0 & 0 & 0 & 0 & \cos\omega t & \sin\omega t & 0 & 0 \\ 0 & 0 & 0 & 0 & -\sin\omega t & \cos\omega t & 0 & 0 \\ 0 & 0 & 0 & 0 & 0 & 0 & \cos\omega t & \sin\omega t \\ 0 & 0 & 0 & 0 & 0 & 0 & -\sin\omega t & \cos\omega t \end{bmatrix}. \tag{5}$$

The mass matrix, stiffness matrix, damping matrix, gyro matrix, and excitation vector of the shaft segment under fixed coordinates are $\mathbf{M}_s^e$, $\mathbf{K}_s^e$, $\mathbf{C}_s^e$, $\mathbf{G}_s^e$, and $\mathbf{F}_s^e$, respectively, as shown in Reference [13]. Because the rotor system structure is axial symmetry, the mass matrix, stiffness matrix, damping matrix, and gyro matrix of the shaft segment under the rotating coordinate are given in Reference [14]:

$$\begin{cases} \mathbf{M}^e = \mathbf{M}_s^e, \\ \mathbf{K}^e = -\omega^2\mathbf{M}_s^e + \omega\mathbf{C}_s^e\mathbf{H} + \mathbf{K}_s^e, \\ \mathbf{C}^e = 2\omega\mathbf{M}_s^e\mathbf{H} + \mathbf{C}_s^e, \\ \mathbf{G}^e = \mathbf{G}_s^e, \\ \mathbf{F}^e = \mathbf{T}'\mathbf{F}_s^e, \end{cases} \tag{6}$$

where $\mathbf{H}$ is the transformation matrix, as follows:

$$\mathbf{H} = \begin{bmatrix} 0 & 1 & 0 & 0 & 0 & 0 & 0 & 0 \\ -1 & 0 & 0 & 0 & 0 & 0 & 0 & 0 \\ 0 & 0 & 0 & 1 & 0 & 0 & 0 & 0 \\ 0 & 0 & -1 & 0 & 0 & 0 & 0 & 0 \\ 0 & 0 & 0 & 0 & 0 & 1 & 0 & 0 \\ 0 & 0 & 0 & 0 & -1 & 0 & 0 & 0 \\ 0 & 0 & 0 & 0 & 0 & 0 & 0 & 1 \\ 0 & 0 & 0 & 0 & 0 & 0 & -1 & 0 \end{bmatrix}. \tag{7}$$

The deep groove ball bearing forces in equation (3) are added, and the motion equation of the whole rotor system in fixed coordinates can be expressed as

$$\begin{aligned} &\mathbf{M}_s\ddot{\mathbf{u}}_s + (\mathbf{C}_s + \mathbf{G}_s)\dot{\mathbf{u}}_s + \mathbf{K}_s\mathbf{u}_s \\ &\quad = \mathbf{F}(\mathbf{t}) + \mathbf{F}_g + \mathbf{N}_g = \mathbf{F}_s, \end{aligned} \tag{8}$$

where $\mathbf{M}_s$, $\mathbf{C}_s$, $\mathbf{G}_s$, and $\mathbf{K}_s$ are the mass matrix, the damping matrix, the gyro matrix, and the stiffness matrix of the rotor system, respectively. $\mathbf{F}(\mathbf{t})$, $\mathbf{F}_g$, and $\mathbf{N}_g$ are unbalanced forces, rolling bearing forces, and gravity at the coupling, bearing, and disk (Y direction), respectively.

The whole finite element matrix of the rotor system is integrated into the group of mass matrix, stiffness matrix, damping matrix, gyro moment, and excitation vector under rotation coordinates. The differential equation of motion of the rotor system under rotational coordinates is

$$\mathbf{M}\ddot{\mathbf{u}} + (\mathbf{C} + \omega\mathbf{G})\dot{\mathbf{u}} + \mathbf{K}\mathbf{u} = \mathbf{F}, \tag{9}$$

where $\mathbf{M}$, $\mathbf{K}$, $\mathbf{C}$, $\mathbf{G}$, and $\mathbf{F}$ are the mass matrix, stiffness matrix, damping matrix, gyro matrix, and excitation vector of the rotor system, respectively. The Rayleigh damping used in the model is

$$\mathbf{C} = \alpha\mathbf{M} + \beta\mathbf{K}, \tag{10}$$

where α is the mass ratio coefficient and β is the stiffness ratio coefficient:

$$\begin{aligned} \alpha &= \frac{2\left(\left(\xi_2/\omega_{n2}\right) - \left(\xi_1/\omega_{n1}\right)\right)}{\left(1/\omega_{n2}^2\right) - \left(1/\omega_{n1}^2\right)}, \\ \beta &= \frac{2\left(\xi_2\omega_{n2} - \xi_1\omega_{n1}\right)}{\omega_{n2}^2 - \omega_{n1}^2}, \end{aligned} \tag{11}$$

where ω_{n1} is the first-order critical speed, ω_{n2} is the second-order critical speed, ξ_1 is the first-order modal damping ratio, and ξ_2 is the second-order modal damping ratio.

In this paper, Newmark-β numerical algorithm and Newton–Raphson iteration are used to solve the nonlinear differential equation (7). Then, the system dynamics analysis is carried out by using the obtained vibration response data of the relevant nodes of the finite element model.

3. Analysis of Dynamic Characteristics of Rotor System with Different Bearing Parameters

The simulation parameters of deep groove ball bearing double-disk rotor system are given as material density of

shaft $\rho = 7850\,\text{kg/m}^3$, elastic modulus $E = 207\,\text{GPa}$, Poisson's ratio $v = 0.3$, the mass of bearing $m_z = 0.5\,\text{kg}$, the mass of coupling $m_c = 0.0439\,\text{kg}$, and the mass of disk $m_d = 0.741\,\text{kg}$. The unbalance is taken as $1.56 \times 10^{-4}\,\text{kg·m}$ and bearing damping $d = 2 \times 10^3\,\text{N/(m/s)}$. According to the simulation parameters, the first- and second-order natural frequencies of the fault rotor system can be determined, respectively, to be $\omega_{n1} = 1750\,\text{r/min}$ and $\omega_{n2} = 6520\,\text{r/min}$.

3.1. Effects of Rotational Speed on Motion Characteristics of Rotor System. The change of speed has the most direct influence on the dynamic characteristics of the rotor system [15]. Figure 4 is a 3D waterfall diagram varying with speed of left bearing (node 7) of the rotor system.

It can be seen that in the speed range of 1000 r/min to 10000 r/min, the main frequency components are rotation frequency (f_r) and VC vibration frequency series (f_{VC}). And in the speed range of 1000 r/min to 6500 r/min, besides rotation frequency (f_r) and VC vibration frequency series (f_{VC}), 1/3 fraction frequency ($1/3f_r$) also occupies a certain frequency proportion, and 2/3 fraction frequency ($2/3f_r$) is not prominent throughout the whole speed range. This kind of harmonic component is mainly caused by the bearing reaction force between the roller and the inner and outer ring of the bearing. The frequency components of $f_{VC} - f_r$ are clearly visible in the speed range of 1000 r/min to 3000 r/min and are no longer apparent as the increase of speed. It is due to the large external excitation produced by the mass unbalance of the rotor system, which weakens the frequency component. From the whole waterfall diagram, the frequency components at most of speeds constitute discrete spectrum, which is also an important feature of the system response in periodic motion. The simulation results in this paper can match the theoretical research results of Reference [11] to a certain extent, which verifies the accuracy of the simulation code.

In order to study the effect of speed on the dynamic characteristics of the rotor system, the vibration response data of the system model's node 7 are extracted to analyze its vibration characteristics theoretically using time domain chart, spectrogram, and Poincaré section.

When the speed is 600 r/min, it can be seen from the spectrogram of Figure 5(b) that in addition to the rotation frequency (f_r), there is also VC vibration frequency series (f_{VC}) and the combined frequency, $f_{VC} + f_r$ and $f_{VC} - f_r$. When the speed continues to increase to 900 r/min, the spectrogram in Figure 6(b) presents a discrete spectrum, and noncommon-divided frequency harmonic component emerges because of the existence of bearing reaction force. 1/2 fraction frequency ($1/2f_r$) appears and the amplitudes of rotation frequency (f_r), VC vibration frequency series (f_{VC}), and the combined frequency are obviously reduced. And the Poincaré section of Figure 6(c) has two periodic attractors. All of these characteristics indicate that the system response is in a state of double period motion, and the system has translated from the motion of period 1 at the speed of 600 r/min to the motion of period 2. From

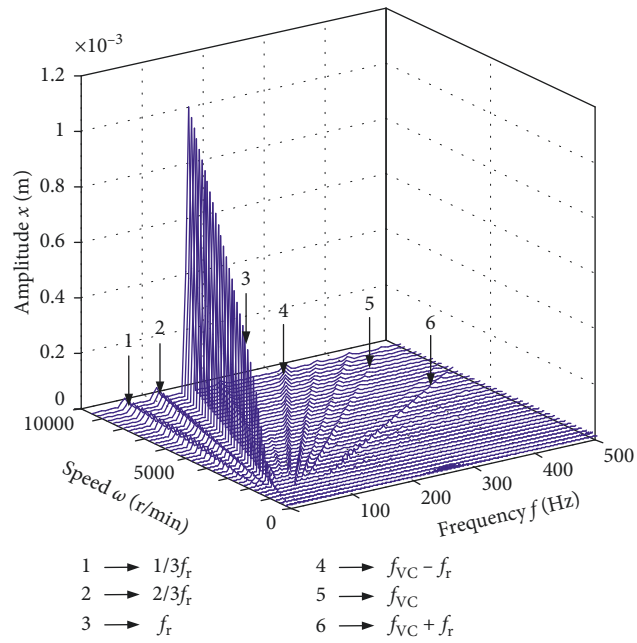

Figure 4: 3D frequency spectrum.

Figures 5(a) and 6(a), the waveform of the system is chaotic and the amplitude varies greatly at low speed. When the speed is further increased to 6000 r/min and 9000 r/min, from Figures 7(b) and 8(b), it is not difficult to see that the vibration amplitude continues to increase and the frequency component occupied by VC vibration frequency series (f_{VC}) and combined frequency is not obvious compared with rotation frequency (f_r). And the time domain charts in Figures 7(a) and 8(a) both present a regular sine curve, and the 1/2 fraction frequency ($1/2f_r$) disappears. The Poincaré mapping presents as a solitary attractor, which explains that the system has been back to the motion state of period 1.

Figure 9 is the displacement vibration amplitude of node 7 varying with rotation speed at X direction and Y direction, respectively. The two lines below represent the maximum and minimum values of the displacement response of the system in the Y direction at different speeds. Similarly, the two lines above represent the maximum and minimum values of the displacement response of the system in the X direction. The larger the amplitude range is, the larger the vibration range of the system is, and the larger vibration range is not conducive to the smooth and effective operation of the rotor system. It can be seen from the figure that because of the influence of gravity at Y direction, the vibration range in Y direction is larger in the process of starting. That is, when the speed is from 0 r/min to 1000 r/min, the range of displacement vibration amplitude at Y direction is larger and shows a decreasing trend. When the speed reaches more than 3000 r/min, the vibration of the rotor system tends to be stable, and the system runs steadily. The fluctuation interval becomes smaller, and it does not decrease with the increase of the speed. In summary, when the rotor is running at low speed, the transverse (X direction) and longitudinal (Y direction)

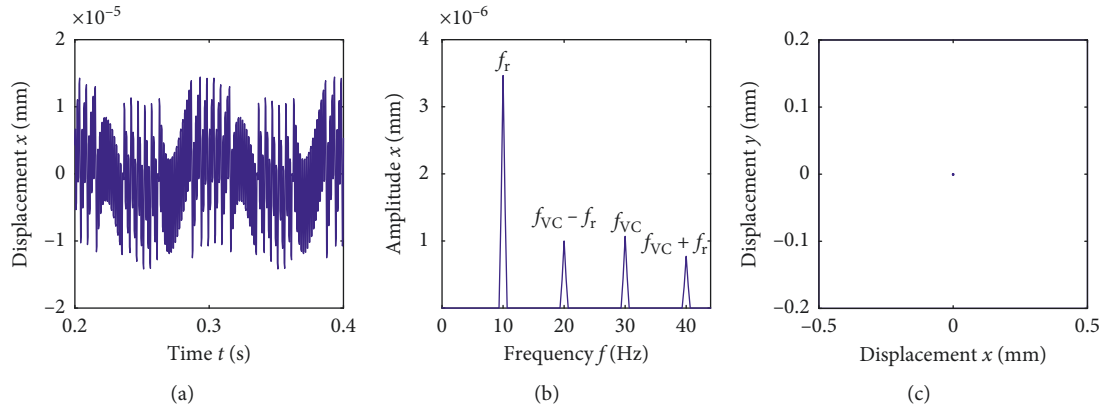

Figure 5: Dynamic response of system at $\omega = 600$ r/min. (a) Waveform. (b) Frequency spectrum. (c) Poincaré map.

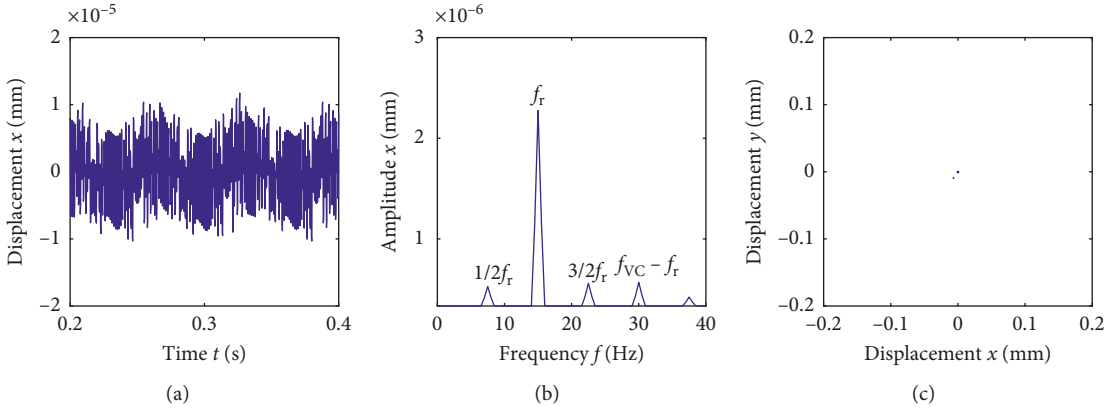

Figure 6: Dynamic response of system at $\omega = 900$ r/min. (a) Waveform. (b) Frequency spectrum. (c) Poincaré map.

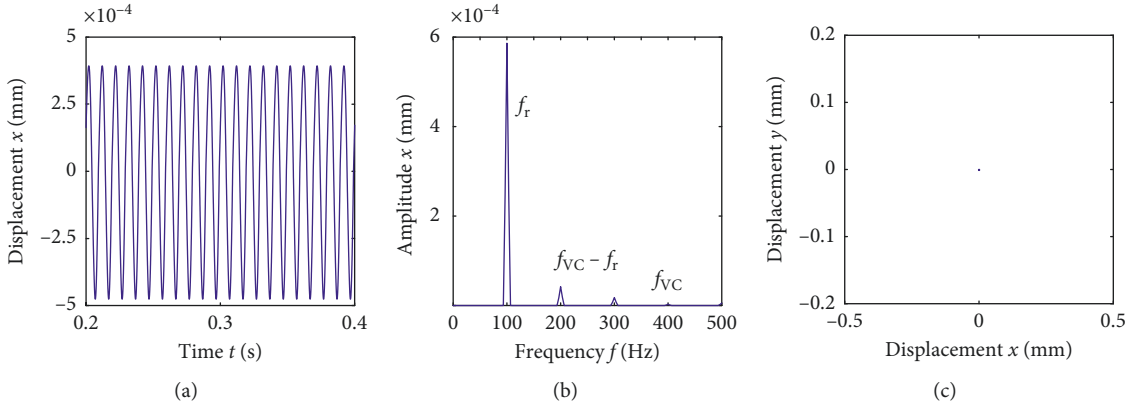

Figure 7: Dynamic response of system at $\omega = 6000$ r/min. (a) Waveform. (b) Frequency spectrum. (c) Poincaré map.

vibration of displacement response are larger, and the VC vibration has a greater impact on the operation stability of the system. In addition, with the increase of the speed, the frequency components except rotation frequency are obviously reduced, and the rotor is running steadily. For the double-disk rotor system supported by the deep groove ball, it is possible to reduce the stable influence of the nonlinear motion characteristic caused by the VC vibration by passing through the low speed zone rapidly.

3.2. Effects of Bearing Clearance on Vibration Response of System. The clearance parameter of rolling bearing is one of the important factors that cause the nonlinearity of rotor

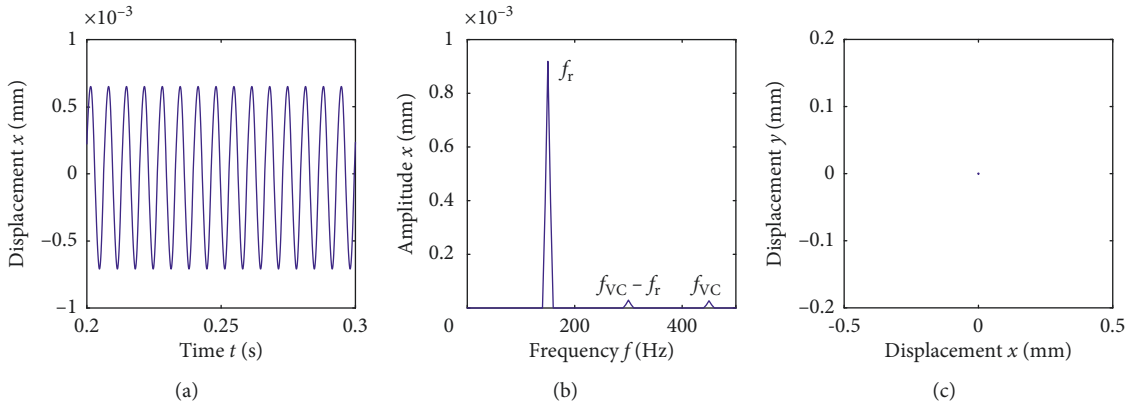

Figure 8: Dynamic response of system at $\omega = 9000$ r/min. (a) Waveform. (b) Frequency spectrum. (c) Poincaré map.

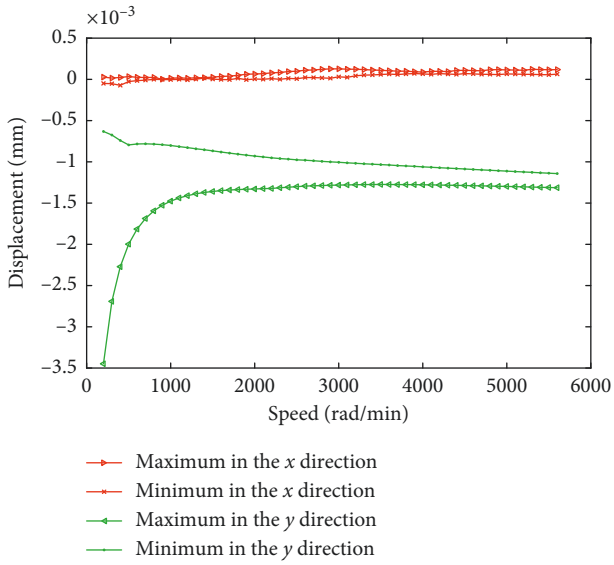

Figure 9: Displacement amplitude at different speeds.

system [16]. The theoretical analysis of the bearing clearance is of great value to the rotor system. It is well known that deep groove ball bearing is a kind of rolling bearings. In order to fully study the influence of clearance parameters on dynamics characteristics of the system, it can be known in Table 2 that the clearance of 61900 deep groove ball bearings is within the range of 0–45 μm. When the speed of the system is under the working conditions, which is between the first and second critical speed, that is, 6000 r/min, the clearance parameters are taken as 4.5×10^{-6} m, 4.5×10^{-9} m, and 4.5×10^{-12} m, respectively. Then, the vibration response curve of the system bearing (node 4) is observed under this large clearance span.

By comparing the time domain charts of Figure 10(a) and Figures 11(a) and 12(a), it is shown that the proper bearing clearance can reduce the vibration amplitude of the system. And from the comparative analysis of the spectrograms of Figure 10(b) and Figures 11(b) and 12(b), the variation of clearance can reduce the proportion of VC vibration frequency series (f_{VC}) and also reduce the influence of nonlinear term on the motion characteristics of the system. Therefore, for deep groove ball bearing double-disk rotor system, the proper bearing clearance value can reduce the vibration amplitude of the system and improve the stability of the rotor system.

3.3. Effects of Bearing Clearance on Vibration Amplitude of the System and Bearing Reaction Force. In order to study the relationship between the vibration amplitude of the bearing (node 4) and the bearing clearance, the bearing clearance is taken as an independent variable, and the vibration amplitude is taken as the dependent variable. The relationship between them is shown in Figure 13. As can be seen from the figure, the vibration amplitude of the node at bearing shows a decreasing trend with the change of clearance. When the clearance is within the range of 0–0.4 μm, the vibration amplitude decreases obviously. When the clearance is within the range of 0.4–2 μm, the vibration amplitude decreases a little more slowly, and when the clearance is within the range of 2–4.5 μm, the vibration amplitude is relatively stable. Thus, too small bearing clearance may lead to the rise of vibration amplitude.

At the same time, the time variation of bearing reaction force under different bearing clearance parameters is also investigated (Figure 14). r_1, r_2, and r_3 in the figure are variation curves of bearing reaction force when the bearing clearance is 4.5×10^{-7} m, 4.5×10^{-8} m, and 4.5×10^{-6} m, respectively. The effect of bearing clearance on bearing reaction force is obvious, which will tend to be stable after 0.1 s, but before 0.1 s, compared to other clearance parameters, the reaction force is more gentle under the clearance parameters of 4.5×10^{-6} m. It can be able to smoothly enter the stable value, and high peak will not appear. The bearing is also less damaged and the fluctuation of bearing reaction force is greater. Therefore, reasonable bearing clearance can not only reduce the vibration amplitude but also protect the bearing outer ring from the irregular impact of the bearing nonlinear reaction force and reduce the damage to the bearings. At the same time, it can also play a positive role to the nonlinear motion characteristics of rotor system.

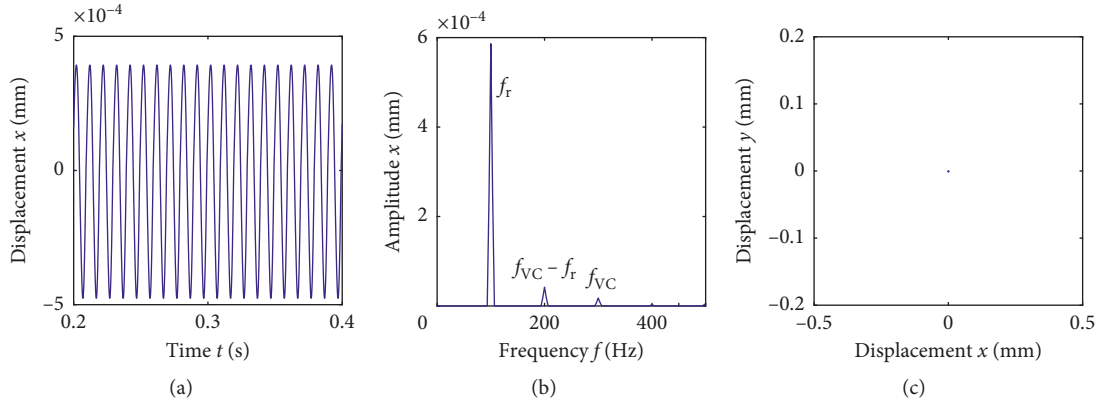

Figure 10: Dynamic response of system at $C = 4.5 \times 10^{-6}$ m. (a) Waveform. (b) Frequency spectrum. (c) Poincaré map.

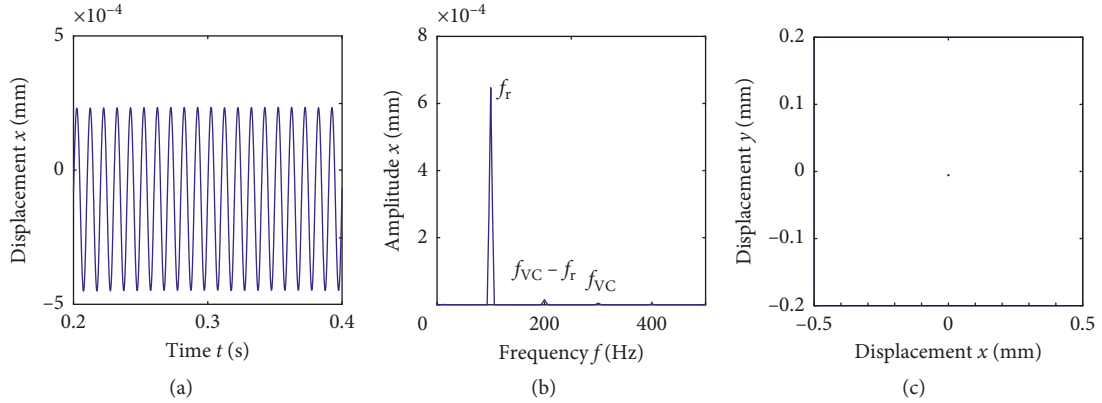

Figure 11: Dynamic response of system at $C = 4.5 \times 10^{-9}$ m. (a) Waveform. (b) Frequency spectrum. (c) Poincaré map.

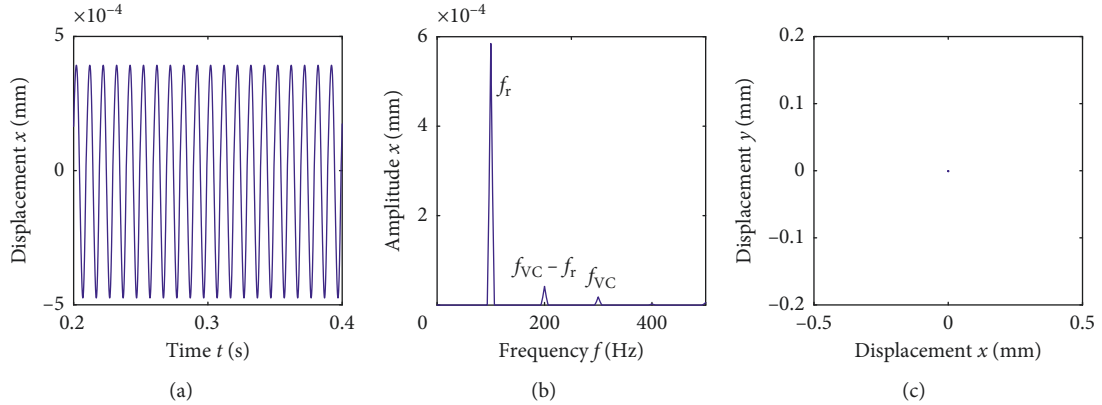

Figure 12: Dynamic response of system at $C = 4.5 \times 10^{-12}$ m. (a) Waveform. (b) Frequency spectrum. (c) Poincaré map.

3.4. Analysis of Acceleration Characteristics of Bearing Inner Ring. The acceleration signal of the inner ring of the bearing (node 4) at X direction is extracted to plot the time variation of the acceleration signal of the bearing inner ring. Figures 15–18 are waveforms under the clearance of 4.5×10^{-6} m, 4.5×10^{-7} m, 4.5×10^{-8} m, and 0 m, respectively. After the accelerated starting area, the waveforms show obvious periodic characteristics.

Contrasting the time domain charts of acceleration signal of bearing inner ring under different bearing clearances, it can be seen that with the decrease of radial clearance, the required time of accelerated starting stage becomes shorter and the acceleration amplitude also increases as the clearance of the bearing decreases. But this regulation will not continue all the time. When the clearance is smaller, even 0 m, the starting time and acceleration amplitude changes little. Therefore, in

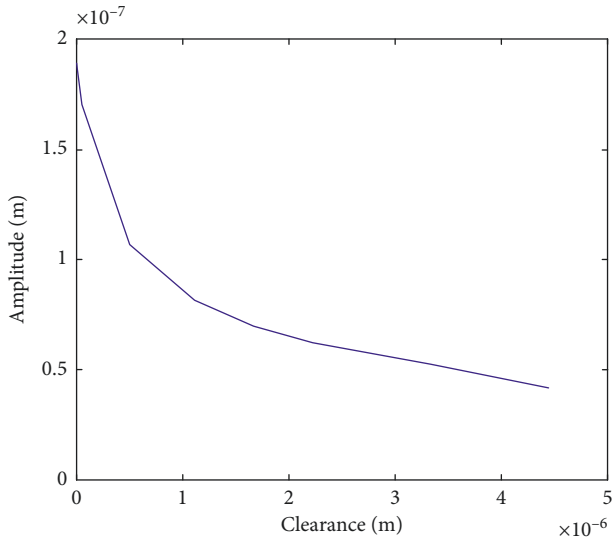

Figure 13: Vibration amplitude-clearance curve at node 4.

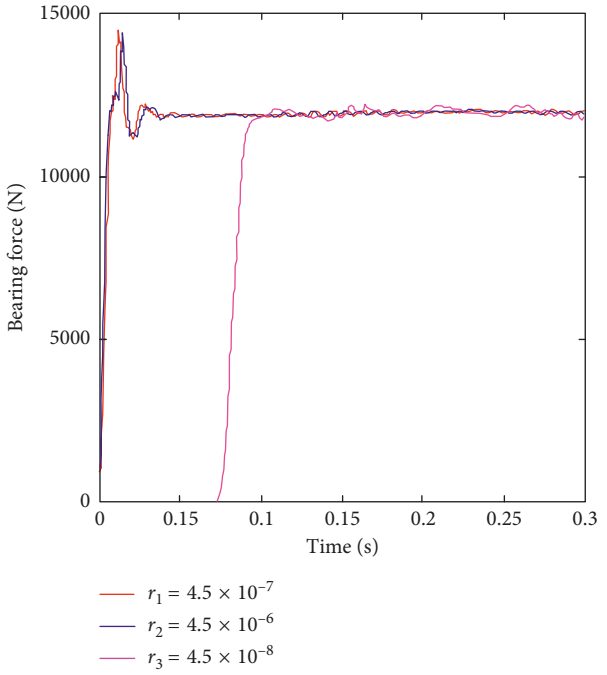

Figure 14: Bearing force curves for different values of the bearing clearance.

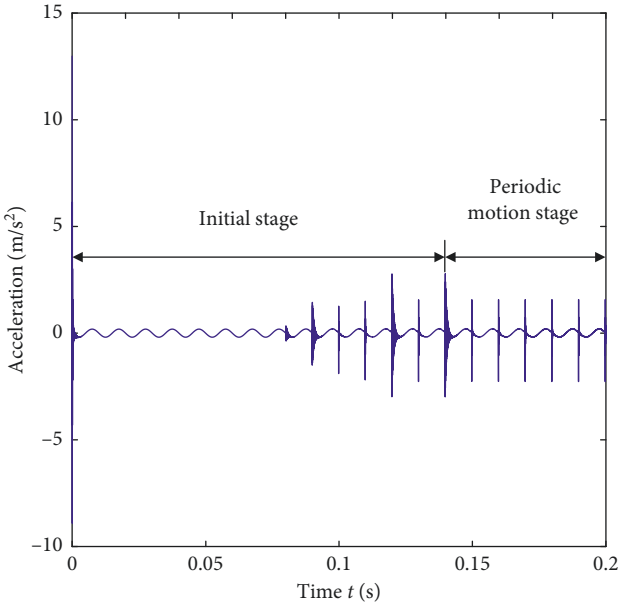

Figure 15: Acceleration curve at clearance $C = 4.5 \times 10^{-6}$ m.

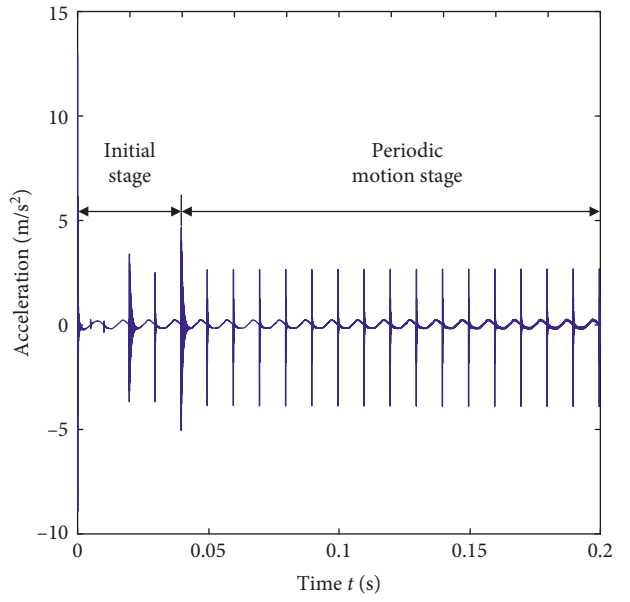

Figure 16: Acceleration curve at clearance $C = 4.5 \times 10^{-7}$ m.

general, bearing clearance of rotor system is directly proportional to the unstable vibration time of accelerated starting stage within certain range.

4. Experiment

According to the theoretical simulation model, bearing seat, shaft, and motor seat are customized according to the ratio of 1 : 1. And the 61900 deep groove ball bearings, rigid copper coupling, and optical flat are purchased to build a test platform. The power of the rotor system is provided by the brushless DC motor whose relevant parameters of the motor are 36VDC, 3600 rpm, and 150 W. The ZM-6610M multifunction controller, which matches the motor, is used to control the motor in order to stabilize the rotating speed. The adjustment of rotating speed can be achieved by changing the resistance of the potentiometer. And the speed of the shaft is displayed by the 5166FR series frequency/tachometer. The vibration form of the axis is measured by using an eddy current displacement sensor of type CWY-DO-502. The data collection for eddy current displacement sensors used the NI-9234 acquisition card and the 8-slot USB cDAQ-9178 crate. Then, the signal will be transferred to the computer via the USB output, and finally the vibration images will be generated using the LabVIEW software. The

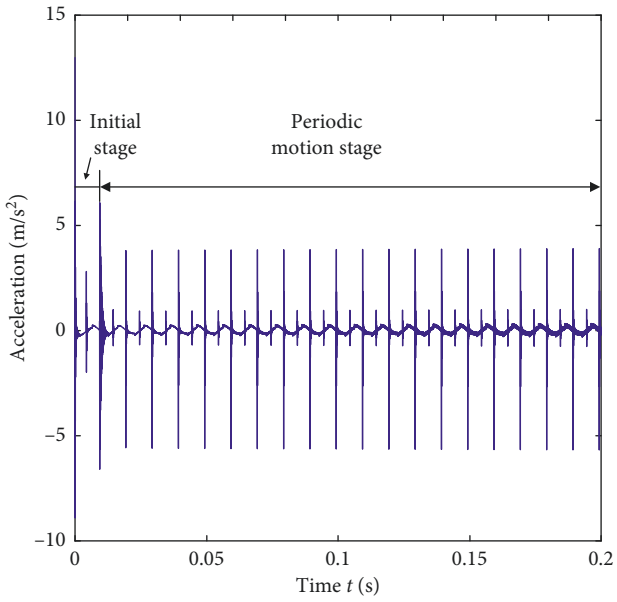

Figure 17: Acceleration curve at clearance $C = 4.5 \times 10^{-8}$ m.

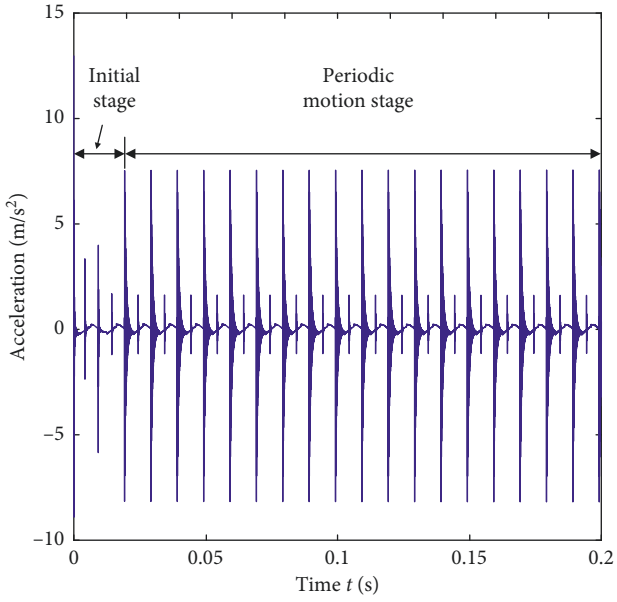

Figure 18: Acceleration curve at clearance $C = 0$.

flow chart of the experiment is given in Figure 19, and the rotor bearing system test rig is shown in Figure 20. The specifications of the experiment apparatus are shown in Table 3.

The three-dimensional spectrum of the measuring point in the vertical direction (X direction) near the right bearing is obtained by the test, as shown in Figure 21. It can be seen that the rotation frequency (f_r) exists simultaneously with the VC vibration frequency series (f_{VC}) in the lower speed range, and their amplitudes are of the same order of magnitude. With the increase of the rotational speed, the amplitude of rotation frequency increases rapidly. Compared with rotation frequency (f_r), the amplitude

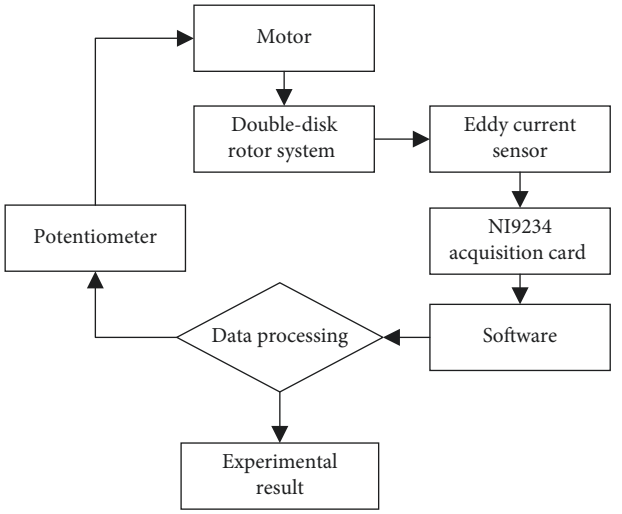

Figure 19: Experimental flow chart.

of the VC vibration frequency series (f_{VC}) decreases gradually, and a small number of fraction frequency components appear. When the speed continues to rise, the amplitude growth rate of rotation frequency gradually slows down and tends to be stable. And the frequency components are more abundant; the components of fraction frequency and VC vibration frequency series (f_{VC}) gradually disappear, and the components of double frequency gradually appear.

The simulation results are compared with the combined frequency characteristics of each speed range obtained by the experiment. The comparison results are shown in Table 4. Comparing the results of experiments and simulations, it can be found that the experimental results are basically consistent with the simulation results in the overall development and evolution trend. But the experimental eccentricity is not completely consistent, and the experimental results are affected by the experimental environment and sensor measurement error, leading to some subbands in the experimental results, dispersing the main frequency energy.

5. Conclusions

(1) When the rotor is in the low speed operation (1000 r/min or less), the VC vibration has a great influence on the motion of the double-disk rotor system supported by the deep groove ball bearings, and it has obvious influence on the amplitude of vibration. As the speed increases to a certain interval, the motion is more stable and the displacement response fluctuates steadily.

(2) Under low speed conditions, the vibration of rotor system displacement is large. With the gradual increase of the rotational speed, the frequency components outside the rotation frequency are significantly reduced, and the operation of the rotor gradually becomes stable. Therefore, for the double-disk rotor system supported by the deep groove ball,

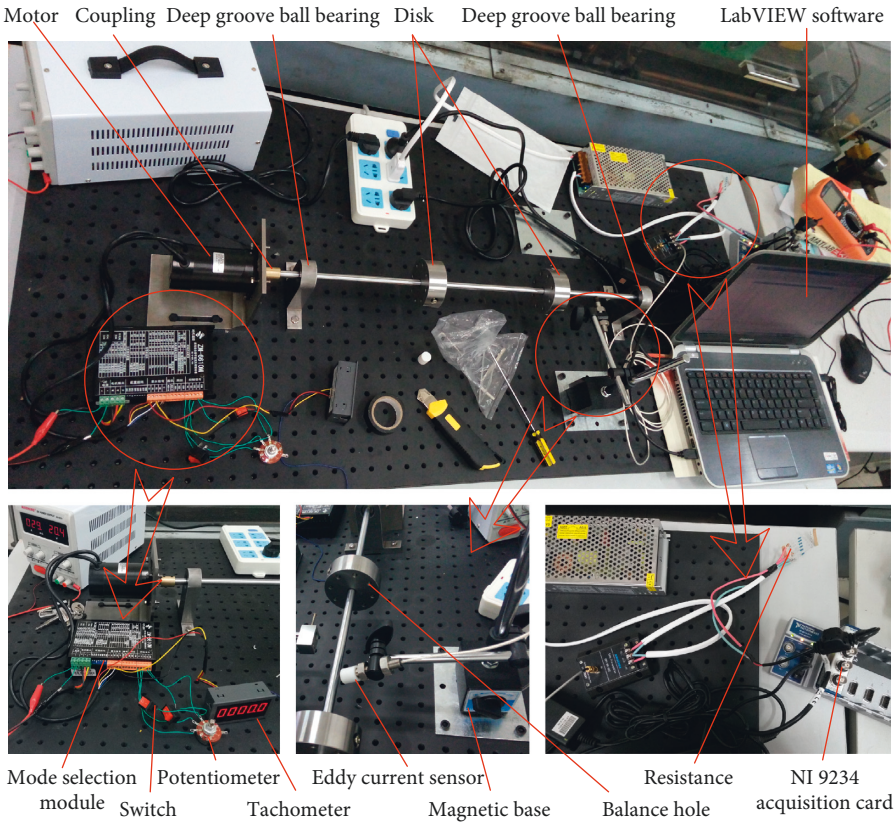

Figure 20: Rotor bearing system test rig.

Table 3: Experiment apparatus.

Experiment apparatus	Specification
Motor	DC 9 V~60 V
Eddy current sensor	CWY-D0-50
Acquisition card	NI-9234
USB chassis	NI cDAQ-9178
Software	LabVIEW

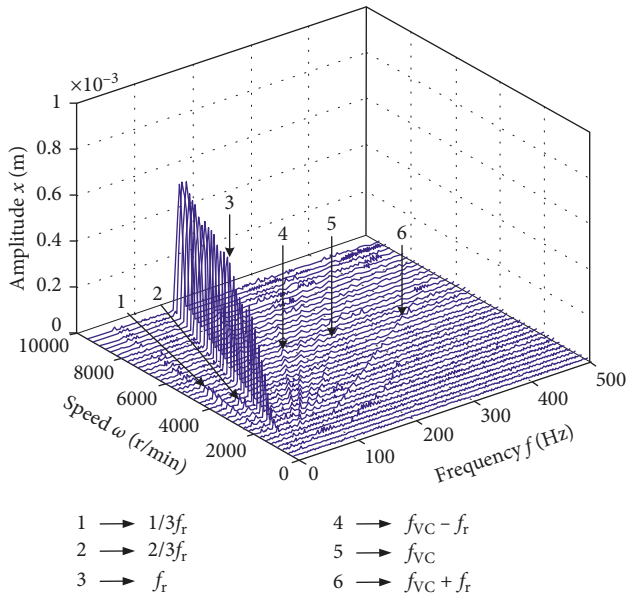

Figure 21: 3D frequency spectrum from experiment.

Table 4: Comparison of frequency components in simulation and test.

	Speed (r/min)	Frequency component
Simulation	$100 \le \omega < 400$	f_r
	$400 \le \omega \le 1\ 760$	$f_r, f_{VC}-f_r, f_{VC}, f_{VC}+f_r$
	$1\ 760 < \omega < 4\ 530$	$1/3f_r, 2/3f_r, f_r, f_{VC}-f_r, f_{VC}, f_{VC}+f_r$
	$4\ 530 \le \omega \le 8\ 420$	$1/3f_r$, $2/3f_r$, f_r, $f_{VC}-f_r$, f_{VC}, $f_{VC}+f_r$, $1/3f_r$ pedigree
	$8\ 420 < \omega < 10\ 000$	$1/3f_r$, $2/3f_r$, f_r, $f_{VC}-f_r$
Test	$100 \le \omega < 280$	f_r
	$280 \le \omega \le 1\ 640$	$f_r, f_{VC}-f_r, f_{VC}, f_{VC}+f_r, f_{VC}+2f_r$
	$1\ 640 < \omega < 4\ 010$	$1/3f_r$, $2/3f_r$, f_r, $f_{VC}-f_r$, f_{VC}, $f_{VC}+f_r$, $f_{VC}+2f_r$
	$4\ 010 \le \omega \le 7\ 730$	$1/3f_r$, $2/3f_r$, f_r, $f_{VC}-f_r$, f_{VC}, $f_{VC}+f_r$, $1/3f_r$ pedigree
	$7\ 730 < \omega < 10\ 000$	f_r, double frequency pedigree

it is possible to reduce the stable influence of the nonlinear motion characteristic caused by the VC vibration by passing through the low speed zone rapidly.

(3) The vibration amplitude of the deep groove ball bearing double-disk rotor system has a strong sensitivity and dependence on the change of bearing clearance. On the one hand, a reasonable bearing clearance can not only reduce the vibration amplitude but also protect the bearing outer ring from the irregular impact of the bearing nonlinear reaction force and reduce the damage to the bearings. On the

other hand, the reasonable bearing clearance can also play a positive role in the nonlinear motion characteristics of the rotor system.

(4) It is found that the larger the bearing clearance, the longer the acceleration start time, the more serious the irregular motion, and the greater impact on the vibration characteristics of the rotor system. The reasonable range of clearance can reduce the effect of unstable motion on the rotor system's vibration characteristics.

Data Availability

The data used to support the findings of this study are included within the article.

Conflicts of Interest

The authors declare that they have no conflicts of interest.

Acknowledgments

This work was financially supported by the General Program of the National Natural Science Foundation of China (Grant nos. 51875093 and U1708257), the Fundamental Research Funds for the Central Universities from Ministry of Education of China (Grant nos. N140304005 and N160313003), and the National Science Foundation for Postdoctoral Scientists of China (Grant nos. 2014M551105 and 2015T80269).

References

[1] H. R. Cao, Y. M. Li, Z. J. He et al., "Time-varying bearing stiffness and vibration response analysis of high speed rolling bearing-rotor system," *Journal of Mechanical Engineering*, vol. 50, no. 15, pp. 73–80, 2014.

[2] A. Gunduz, J. T. Dreyer, and R. Singh, "Effect of bearing preloads on the modal characteristics of a shaft-bearing assembly: experiments on double row angular contact ball bearings," *Mechanical Systems and Signal Processing*, vol. 31, no. 6, pp. 176–195, 2012.

[3] J. P. Chavez and M. Wiercigroch, "Bifurcation analysis of periodic orbits of a non-smooth Jeffcott rotor model," *Communications in Nonlinear Science and Numerical Simulation*, vol. 18, no. 9, pp. 2571–2580, 2013.

[4] S. Fukata, E. H. Gad, T. Kondou, T. Ayabe, and H. Tamura, "On the radial vibration of ball bearings: computer simulation," *Bulletin of JSME*, vol. 28, no. 239, pp. 899–904, 1985.

[5] B. Mevel and J. L. Guyader, "Routes to chaos in ball bearings," *Journal of Sound and Vibration*, vol. 162, no. 3, pp. 471–487, 1993.

[6] F. Cong, J. Chen, G. Dong, and M. Pecht, "Vibration model of rolling element bearings in a rotor-bearing system for fault diagnosis," *Journal of Sound and Vibration*, vol. 332, no. 8, pp. 2081–2097, 2013.

[7] Y. B. Kim and S. T. Noah, "Quasi-periodic response and stability analysis for a non-linear Jeffcott rotor," *Journal of Sound and Vibration*, vol. 190, no. 2, pp. 239–253, 1996.

[8] H. L. Zhou and G. Chen, "Dynamic response analysis of dual rotor-ball bearing-stator coupling system for aero-engine," *Journal of Aerospace Power*, vol. 24, no. 6, pp. 1284–1291, 2009, in Chinese.

[9] M. Tiwari, K. Gupta, and O. Prakash, "Dynamic response of an unbalanced rotor supported on ball bearings," *Journal of Sound and Vibration*, vol. 238, no. 5, pp. 757–779, 2000.

[10] F. M. A. El-Saeidy, "Time-varying total stiffness matrix of a rigid machine spindle-angular contact ball bearings assembly: theory and analytical/experimental verifications," *Shock and Vibration*, vol. 18, no. 5, pp. 641–670, 2011.

[11] G. Chen, "Rotor-ball bearing-stator coupling dynamic model including rubbing coupling faults," *Journal of Vibration Engineering*, vol. 20, no. 4, pp. 361–368, 2007, in Chinese.

[12] F. Kong, W. Huang, Y. Jiang, W. Wang, and X. Zhao, "A vibration model of ball bearings with a localized defect based on the hertzian contact stress distribution," *Shock and Vibration*, vol. 2018, Article ID 5424875, 14 pages, 2018.

[13] Q. K. Han, T. Yu, D. W. Wang et al., *Nonlinear Vibration Analysis and Diagnosis of Faulted Rotor System*, Science Press, Beijing, China, 2010, in Chinese.

[14] A. Nandi, "Reduction of finite element equations for a rotor model on non-isotropic spring support in a rotating frame," *Finite Elements in Analysis and Design*, vol. 40, no. 9-10, pp. 935–952, 2004.

[15] W. M. Wang, P. Y. Qi, Q. X. Li et al., "Instability control strategy for rotor-bearing system in centrifugal compressor," *Vibration and Shock*, vol. 33, no. 6, pp. 102–106, 2014, in Chinese.

[16] S. T. Zhou, H. G. Li, L. Zhang et al., "Stochastic unbalance response characteristics of rotor systems based on intrusive spectral stochastic finite element method," *Vibration and Shock*, vol. 35, no. 19, pp. 45–49, 2016, in Chinese.